Effects of Strain Rate on Tensile Behavior of Reactive Powder Concrete

Kazunori Fujikake[1], Takanori Senga[2], Nobuhito Ueda[3], Tomonori Ohno[4] and Makoto Katagiri[5]

Abstract

Reactive Powder Concrete (RPC) reinforced with short steel fibers is characterized by ultra-high strength and high fracture toughness. Because of its excellent properties, RPC may be suitable as an advanced material for reinforced concrete structures subjected to impact loading. Thus, the objective of this study was to find out the effects of strain rates on tensile behaviors of RPC specimens subjected to rapid loading. The influence of the loading rates on failure modes, tensile stress-elongation curves and tensile stress-crack opening curves was investigated. Furthermore, based on the test results, a rate-dependent bridging law expressing the relation between tensile stress and crack opening was proposed.

1. Introduction

Reactive Powder Concrete (RPC), which was developed in France in the 1990s, is a special type of ultra-high strength cementitious composite reinforced with short steel fibers (Cheyrezy *et al*. 1995, Richard and Cheyrezy 1995). It is characterized by an ultra-high compressive strength in excess of 200 MPa, very high ductility and extremely low permeability, creep and shrinkage. These characteristics are obtained by eliminating large aggregate, including large quantities of superplasticizer and silica fume, optimizing the packing density of fine particles, introducing short steel fibers and applying heat curing.

While RPC has already been applied to several pedestrian bridges, its ultra-high strength and very high toughness make it potentially highly suitable for structures that need to resist impact loading caused by crashing vehicles, ships or airplanes, falling rocks, avalanches or explosions. Impact loading is generally an extremely severe loading condition, characterized by great intensity and short duration. Many previous research projects have highlighted the effectiveness of conventional fiber reinforced concrete under impact loading (Naaman and Gopalaratnam 1983, Gopalaratnam and Shah 1986, Banthia *et al*. 1996, Bindiganavile and Banthia 2001). However, less information on the impact behavior of ultra-high strength fiber reinforced concrete is available (Bindiganavile *et al*. 2002).

[1]Associate Professor, Department of Civil and Environmental Engineering, National Defense Academy, Japan.
E-mail: fujikake@nda.ac.jp
[2]Officer, Ground Self-Defense Force, Japan.
[3]Research Engineer, Research & Development Center of Taiheiyo Cement Corporation, Japan.
[4]Professor, Department of Civil and Environmental Engineering, National Defense Academy, Japan.
[5]Manager, Research & Development Center of Taiheiyo Cement Corporation, Japan.

To assess the application of RPC to RC structures subjected to impact loads, the dynamic mechanical properties of RPC under high strain-rates are essential. Fujikake *et al*. (2002) have examined the dynamic behaviors of RPC material subjected to high strain-rates and triaxial compressive stresses. However, very little is known about the response of RPC material subjected to rapid tensile loading. Therefore, the aim of this study is to investigate the effect of loading rate on the mechanical properties of RPC specimens subjected to uniaxial rapid tensile loading.

2. Experimental program

2.1 Test specimens

The prismatic specimens used had a cross-sectional dimension of 50×50 mm and a length of 100 mm as shown in **Fig. 1**. To predetermine the fracture location of the specimen, a notch (12.5 mm deep and 3 mm wide) was inserted at the center of the specimen on two sides. The notch depth was determined by preliminary tests in which the influence of notch depth sizes on maximum tensile loads and stresses was examined under static loading. From the preliminary test result shown in **Fig. 2**, while the maximum tensile load decreases with increases in notch depth, the maximum tensile strength evaluated with a net cross-sectional area at the notch section is identical.

Bonded steel end plates were used to apply rapid tensile load to the specimen as shown in **Fig. 3**. The steel end plate had a cross-sectional dimension of 70×70 mm and a thickness of 35 mm. An epoxy adhesive was used to glue the steel end plate to the specimen. When applying the epoxy adhesive, the bonded surface between the steel end plate and the specimen was subjected to a compressive pressure of 0.5 MPa. The epoxy adhesive was generally controlled to be approximately 0.5 to 1.0 mm thick. The assembly was cured for more than two days for the epoxy adhesive to develop strength.

2.2 Material compositions and properties

Table 1 details the mix proportion used in this study.
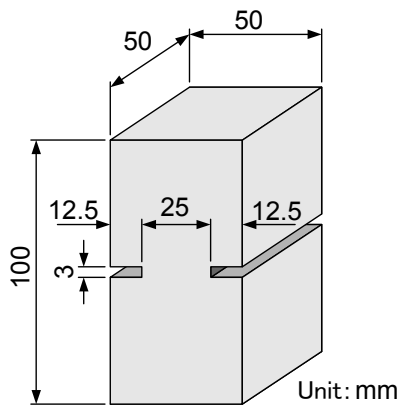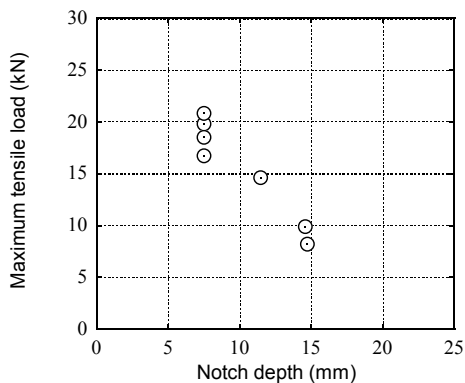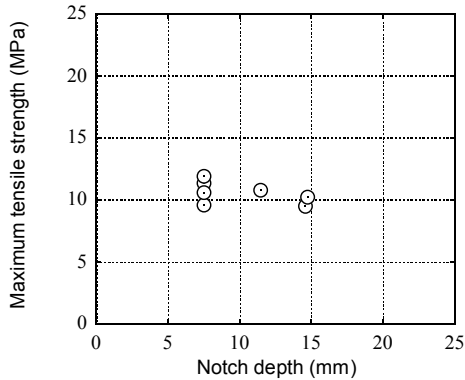
Fig. 1 Prismatic specimen.

(a) Maximum tensile load vs. notch depth

(b) Maximum tensile strength vs. notch depth

Fig. 2 Preliminary test result.

Fig. 3 Detail of specimen fixing.

Table 1 Mix proportion.

Fiber volume fraction V_f (%)	2.0
Water-cement ratio W/C (%)	22.0
Water*1 (kg/m^3)	180
Premix pre-blended powders (kg/m^3)	2254
Steel fiber (kg/m^3)	157
Superplasticizer (kg/m^3)	25

*1 including superplasticizer

Table 2 Mechanical properties of RPC under static loading.

Compressive strength	214.7 MPa
Flexural strength	40.0 MPa
Youngs modulus	55 GPa
Poisson ratio	0.2

Pre-blended powders, provided as Ductal Premix on a commercial basis, consist of Portland cement, silica fume, quartz sand with a maximum particle diameter of 1.2 mm used as fine aggregate and very fine powder composed mainly of quartz as the mineral admixture. Two percent of short straight steel fibers in volume were introduced to the mix. The steel fibers used were 15 mm long, with a diameter of 0.2 mm. The specimens were cast horizontally in wooden molds. After removal from the molds, all specimens were cured at 90℃ for 2 days. The mechanical properties of RPC in a uniaxial static compression test are given in **Table 2**.
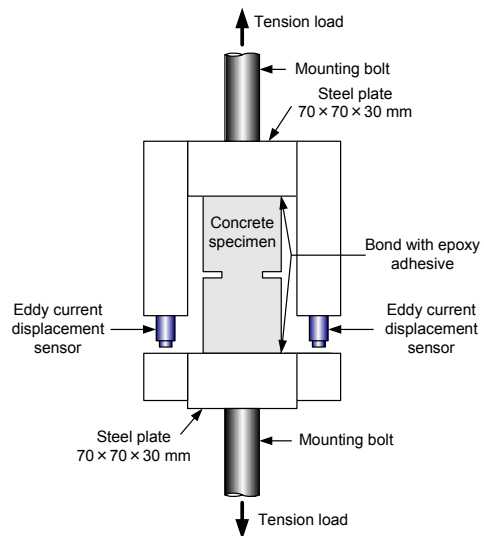
2.3 Test procedure
The uniaxial rapid tensile loading system that was used consisted of a uniaxial tensile loading apparatus and a servo-controlled rapid loading machine with a maximum loading capacity of 980 kN and a maximum loading speed of 4 m/s as shown in **Fig. 4**.

The upper and lower sides of the specimen were rigidly attached to a firmly fixed load cell and to a movable loading frame, respectively, through bolts in the uniaxial loading apparatus, thereby restraining the end rotations of the specimen. Tensile loads were applied to the specimens by moving the loading frame downward at the specified rates under displacement control. Four loading rates of 1.0×10^{-4}, 2.0×10^{-1}, 2.0×10^{0} and 5.0×10^{1} (mm/s) were adopted. These rates are referred to as static, low-rate, medium-rate, high-rate loading in this paper, respectively. Three specimens were tested at each loading rate.
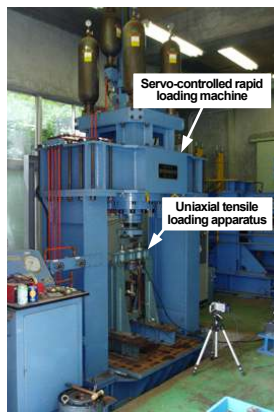
(a) Servo-controlled rapid loading machine and uniaxial tensile loading apparatus
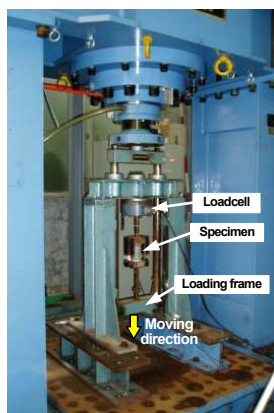
(b) Uniaxial tensile loading apparatus

Fig. 4 Uniaxial rapid loading system.

2.4 Measurement

In the uniaxial rapid tensile loading test, an overall elongation of the specimen was measured by a pair of eddy current displacement sensors mounted on both sides of the specimen as shown in **Fig. 3**. The load acting on the specimen was measured using a loadcell as shown in **Fig. 4**.

3. Experimental results and discussion

3.1 Failure modes

All specimens failed at one major crack in a direction almost perpendicular to the loading axis as shown in **Fig. 5**. The fracture planes formed shared a similar appearance in which the steel fibers were completely pulled out on either side of the fracture planes, regardless of the loading rate.

3.2 Influence of loading rates on tensile stress - elongation relationships

Figure 6 shows typical tensile stress-elongation relationships obtained in the uniaxial rapid tensile loading test. The tensile stress was calculated as a mean stress with a net cross-sectional area considering the notches. RPC is shown to initially respond in an essentially elastic manner up to a certain stress level. When the tensile stress reaches the first cracking strength at which the

(a) Static loading   (b) Low-rate loading

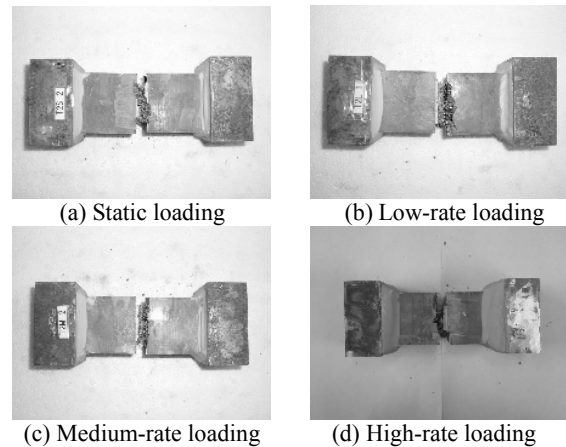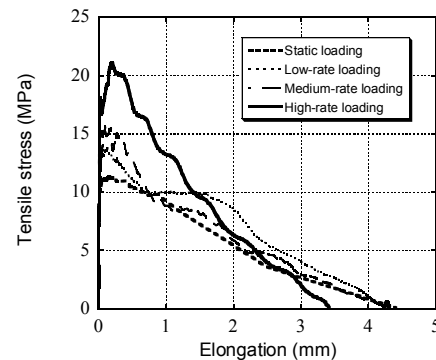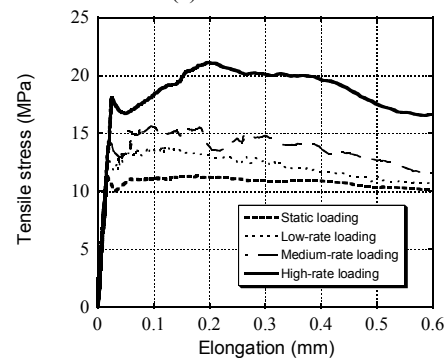(c) Medium-rate loading   (d) High-rate loading

Fig. 5 Typical failure mode.

(a) Entire curve

(b) Close-up of lower elongation region

Fig. 6 Tensile stress-elongation relation.

matrix begins to crack, the tensile stress-elongation curve departs from linearity. After the first cracking strength, the tensile stress slightly increases up to the maximum tensile strength, although the relative strength increase is less significant. Both the first cracking and maximum tensile strengths increase with increases in loading rate, while the initial slopes of the curves are identical regardless of the loading rates. The elastic modulus evaluated from the tensile stress-elongation relations is approx. 60 GPa. Beyond the displacement of 2.0 mm, the tensile stress-elongation curve for dynamic loading approximates the curve for static loading.

3.3 Tensile stress-crack opening

Hillerborg *et al*. (1976) first proposed a fictitious crack model for tensile fractures of concrete. In that model, a tensile stress-crack opening relation was considered as a unique material property in the post-peak region. Currently many design codes adopt the stress-crack opening expression for tension fracture of concrete (CEB-FIP 1990, JSCE 2002). Thus, it is significant to investigate the tensile stress-crack opening curve for RPC material under rapid tensile loading.

To calculate a crack opening for the measured elongation, it is assumed that the crack opening is zero at the first cracking strength and that beyond the first cracking strength, the uncracked parts of the specimen behaves as an elastic material with initial elastic modulus E_0. Thus, as shown in **Fig. 7**, the crack opening at a point B is given as follows:

$$w_c = \delta - \delta_e = \delta - \frac{\sigma}{K} \tag{1}$$

where δ : overall elongation of the specimen, δ_e : elastic elongation component at a point B, K : elastic stiffness given as $K = E/L$.

Figure 8 shows typical tensile stress-crack opening relations obtained from the uniaxial rapid tensile loading test. As previously mentioned, after the first cracking strength, the tensile stress slightly increases up to the maximum strength. The difference between the first cracking strength and the maximum tensile strength tends to increase with increases in loading rate. This is probably due to the improvement in interfacial bond between the matrix and steel fiber through the loading rate effect. However, at the crack opening of 0.4 mm or less, the tensile stress is rationally regarded as a constant at each loading rate. Thus, average tensile strengths at the crack opening of 0.4 mm or less are calculated as shown in **Table 3**. In the later discussion, the average tensile strength for each loading rate is called a dynamic tensile strength for convenience and that for static loading is only called a static tensile strength. While the crack opening is greater than 0.4 mm, the tensile stress decreases with increases in the crack opening. Beyond the crack opening of 2.0 mm, the tensile stress-crack opening curves are identical, regardless of the loading rate.

The relation between the dynamic tensile strength and the loading rate was examined and formulated. In the formulation, since the strain distribution of the specimen was uniform without localization before reaching the maximum strength, it was efficient to express the loading rates with a strain rate. The corresponding strain rates of static, low-rate, medium-rate, high-rate loadings were 1.0×10^{-6}, 2.0×10^{-3}, 2.0×10^{-2}, 5.0×10^{-1} /s, respectively. **Figure 9** shows the dynamic tensile strength-strain rate relation. The dynamic tensile strength increases by 70% as the strain rate increases from 1.0×10^{-6} to 5.0×10^{-1}/s. The dynamic tensile strength is given as:

(a) Tensile stress-elongation relation

(b) Tensile stress-crack opening relation

Fig. 7 Calculation for crack opening.
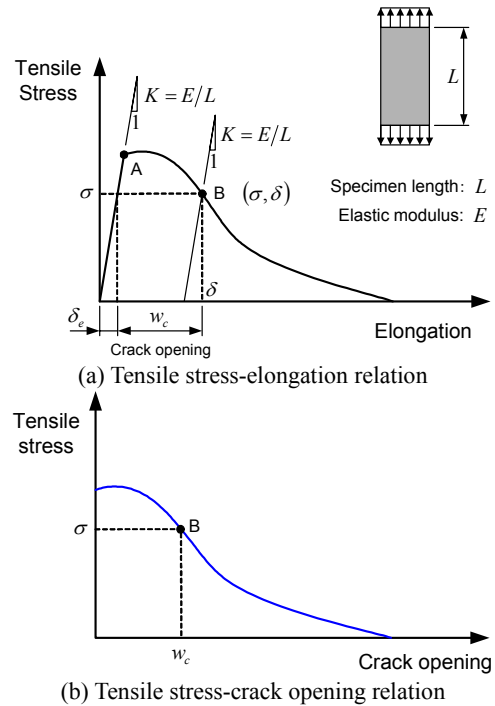

(a) Entire curve
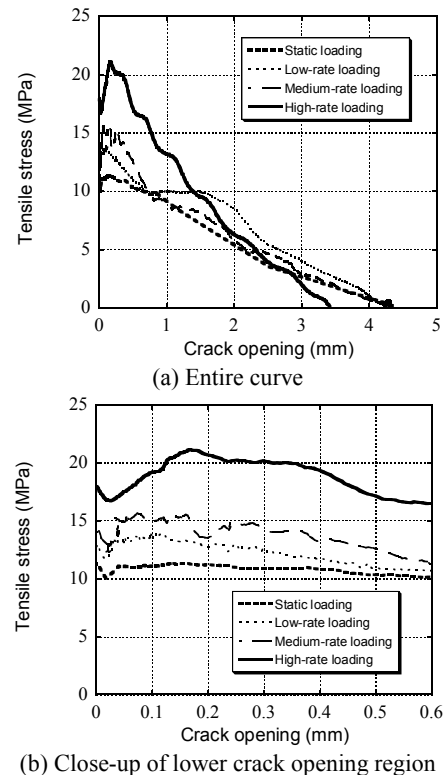

(b) Close-up of lower crack opening region

Fig. 8 Tensile stress-crack opening curve.

$$f_{tf,d} = f_{tf,s} \left(\frac{\dot{\varepsilon}}{\dot{\varepsilon}_{st}} \right)^{0.0013 \left[Log \left(\frac{\dot{\varepsilon}}{\dot{\varepsilon}_{st}} \right) \right]^{1.95}} \tag{2}$$

Table 3 First cracking strength and max. tensile strength.

Loading rate (mm/s)	Test No.	First cracking strength (MPa)	Max. tensile strength		Ave. Tensile strength up to crack opening of 0.4 mm (MPa)
			Strength (MPa)	Corresponding crack opening (mm)	
1.0×10^{-4} (Static)	1	11.29	11.34	0.162	10.98
	2	11.91	11.91	0.0	11.22
	3	10.46	10.58	0.108	10.07
2.0×10^{-1} (Low-rate)	1	11.53	11.77	0.134	11.20
	2	12.85	13.86	0.099	12.74
	3	14.59	14.80	0.069	12.71
2.0×10^{0} (Medium-rate)	1	11.34	13.29	0.138	12.11
	2	14.42	15.63	0.073	14.41
	3	14.83	15.30	0.118	13.47
5.0×10^{1} (High-rate)	1	16.65	17.78	0.206	16.50
	2	18.04	21.12	0.168	19.55
	3	17.65	19.92	0.124	18.67
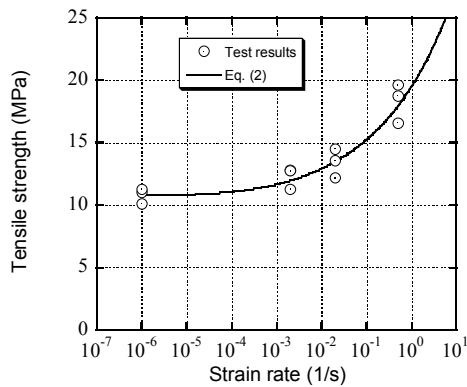
Fig. 9 Dynamic tensile strength-strain rate relationship.

Fig. 10 Trilinear curve for tensile stress-crack opening relation.

where $f_{tf,s}$: static tensile strength = 10.8 MPa, $\dot{\varepsilon}_{st}$: strain rate corresponding to static loading = 1.0×10^{-6} /s. The dynamic tensile strength calculated by Eq. (2) is shown in **Fig. 9**.

Based on the test results, the trilinear curve shown in **Fig. 10** was adopted to express the tensile stress-crack opening relationship. Therefore, the tensile stress-crack opening relationship is given as:

$$\sigma(w_c) = \begin{cases} f_{tf,d} & \text{for } 0 \leq w_c \leq w_1 \\ f_{tf,d} - \dfrac{f_{tf,d} - \sigma_2}{w_2 - w_1}(w_c - w_1) & \text{for } w_1 < w_c \leq w_2 \\ \sigma_2 - \dfrac{\sigma_2}{w_3 - w_2}(w_c - w_2) & \text{for } w_2 < w_c \leq w_3 \end{cases}$$

(3)

The tensile stress-crack opening relationships given by Eq. (3) for the static, the low-rate, the medium-rate and the high-rate loadings are shown in **Fig. 11**.

4. Conclusions
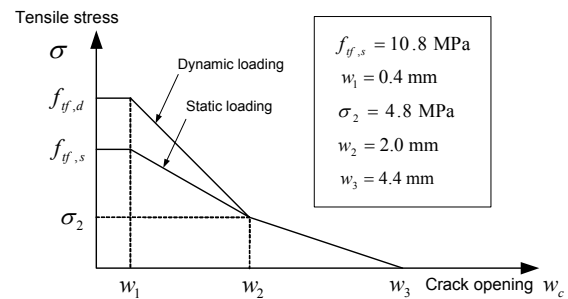
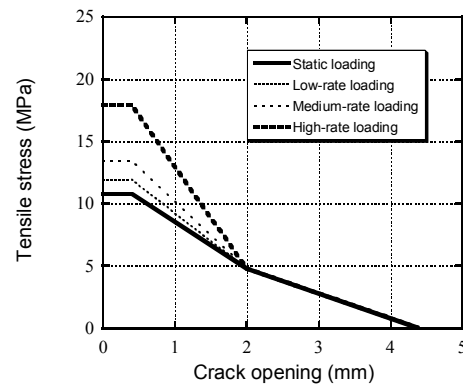Based on the results presented in this paper, the follow-

Fig. 11 Calculated tensile stress-crack opening relation.

ing conclusions can be drawn.
(1) RPC behaved as an elastic material up to the first cracking strength. The elastic modulus was identical regardless of the loading rate.
(2) The tensile stress at the crack opening range of 0 to 0.4 mm was approximately constant.
(3) The relation between the tensile stress and crack opening was formulated to consider the strain rate effect.
(4) The tensile stress-crack opening curves for crack openings greater than 2.0 were identical, regardless

of the loading rate.
(5)   The tensile stress-crack opening curve fits well with a trilinear curve.

References

Banthia, N., Mindess, S. and Trottier, J.-F. (1996). "Impact resistance of steel fiber reinforced concrete." *ACI Materials Journal*, 93 (5), 472-479.

Bindiganavile, V. and Banthia, N. (2001). "Polymer and steel fiber-reinforced cementitious composites under impact loading—Part 2: Flexural toughness." *ACI Materials Journal*, 98 (1), 17-24.

Bindiganavile, V., Banthia, N. and Aarup, B. (2002). "Impact response of ultra-high-strength fiber-reinforced cement composite." *ACI Materials Journal*, 99 (6), 543-548.

CEB-FIP (1990). "*CEB-FIP MODEL CODE 1990.*" First Draft, CEB Bulletin d'Information No. 195.

Cheyrezy, M., Maret, V. and Frouin, L. (1995). "Microstructural analysis of RPC (Reactive Powder Concrete)", *Cement and Concrete Research*, 25 (7), 1491-1510.

Fujikake, K., Uebayashi, K., Ohno, T., Shimoyama, Y. and Katagiri, M. (2002). "Dynamic properties of steel fiber reinforced mortar under high-rates of loadings and triaxial stress states." *In:* N. Jones, C. A. Brebbia, and A. M. Rajendran, Eds., *Proceedings of the 7th International Conference on Structures Under Shock and Impact, Montreal*, WIT Press, 437-446.

Gopalaratnam, V. S. and Shah, S. P. (1986). "Properties of steel fiber reinforced concrete subjected to impact loading." *ACI Journal*, 83 (1), 117-126.

Hillerborg, A., Modeer, M. and Petersson, P. E. (1976). "Analysis of crack formation and crack growth in concrete by means of fracture mechanics and finite elements." *Cement and Concrete Research*, 6, 773-782.

JSCE (2002). "*Standard Specifications for Concrete Structures-2002, Structural Performance Verification.*"

Naaman, A. E. and Gopalaratnam, V. S. (1983). "Impact properties of steel fiber reinforced concrete in bending." *International Journal of Cement Composites and Lightweight Concrete*, 5 (4), 225-237.

Richard, P. and Cheyrezy, M. (1995). "Composition of reactive powder concretes." *Cement and Concrete Research*, 25 (7), 1501-1511.